Unconventional superconductivity of an altermagnetic metal: Polarized BCS and inhomogeneous Fulde-Ferrell-Larkin-Ovchinnikov states

Hui Hu,¹ Zhao Liu,¹ and Xia-Ji Liu¹

¹Centre for Quantum Technology Theory, Swinburne University of Technology, Melbourne 3122, Australia (Dated: May 19, 2025)

We investigate the superconductivity of two-dimensional spin-1/2 Fermi systems with d-wave altermagnetism under external magnetic field near zero temperature. At large altermagnetic coupling without magnetic field, we show that altermagnetism drives a second-order phase transition from the standard Bardeen-Cooper-Schrieffer (BCS) state to an inhomogeneous Fulde-Ferrell-Larkin-Ovchinnikov (FFLO) state. The inclusion of magnetic field turns the BCS state into a long-sought polarized BCS superconductor with spin-population imbalance. It also shrinks the parameter window of the FFLO state and eventually leads to a nontrivial quantum tri-critical Lifshitz point, where two second-order phase transition lines between the polarized BCS, FFLO and normal states intersect. At small altermagnetic coupling, we find the usual route to the FFLO state driven by magnetic field. The presence of the altermagnetic coupling narrows the phase window of the FFLO state and creates another quantum Lifshitz point, where a first-order transition curve meets a second-order transition line. Between the two Lifshitz points, the transition from the polarized BCS state to the normal state is smooth. Our predicted rich phase diagram is relevant to some recently discovered unconventional magnets, including RuO₂ that exhibits a relatively high superconducting temperature in the thin film limit under applied strain. Our results of unconventional superfluidity are also testable in ultracold atom laboratories, where a spin-1/2 altermagnetic Fermi gas might be realizable upon loading into two-dimensional Hubbard lattices.

I. INTRODUCTION

At absolute zero temperature, the possibility of superconductivity or superfluidity in spin-population imbalanced interacting Fermi systems remains elusive¹⁻⁴. The best known theoretical proposal is the so-called Fulde-Ferrell-Larkin-Ovchinnikov (FFLO) state driven by an external magnetic field, as independently suggested by Fulde and Ferrell (FF)⁵ and by Larkin and Ovchinnikov (LO)⁶ in 1960s. In the FFLO state, Cooper pairs carry a nonzero center-of-mass momentum due to the mismatched Fermi surfaces for each spin component. As a result, the pairing order parameter becomes spatially inhomogeneous. However, despite enormous efforts in theory and experiment over the past six $decades^{7-22}$, there is so far no smoking-gun evidence that such an exotic finitemomentum superconductor has been observed. The second best known candidate of imbalanced superconductivity is probably the Sarma state²³ or the breached pairing state²⁴, which condensates at zero momentum. This polarized, BCS like state typically corresponds to a local maximum in the energy landscape, and therefore requires some very specified conditions to thermodynamically stabilize 25,26 .

Most recently, in a pioneering study²⁷ Chakraborty and Black-Schaffer surprisingly suggested that a FFLO state can be induced by d-wave altermagnetism in the absence of magnetic field in the newly discovered altermagnetic metals^{28–37}. Although there is no net magnetism due to the unconventional, momentum-dependent form of the collinear magnetic order³³, the FFLO state was predicted to arise in the presence of an attractive d-wave interaction potential²⁷. This interesting finding was attributed to the d-wave symmetry of the supercon-

ducting order parameter whose gapless nodes coincide with the altermagnetic nodes. The FFLO state disappears for an s-wave interaction potential 27 . On the other hand, the altermagnetism induced FFLO state was found to smoothly connect the magnetic field induced FFLO state²⁷. Therefore, the transition from the BCS state to the FFLO state, induced by either altermagnetism or magnetic field, is first order. However, in a subsequent research by Hong, Park and Kim³⁸, it was clearly demonstrated that an s-wave on-site interaction can accommodate the FFLO state at a fixed chemical potential, through the formation of Bogoliubov Fermi surface. Moreover, the transition from the BCS state to the altermagnetism induced FFO state is smooth³⁸. To reconcile the two controversial observations, on the stabilization mechanism of the FFLO state and on the order of the phase transition, clearly we need more in-depth exploration of the altermagnetism induced FFLO state.

We note that, the finite-momentum Cooper pairing³⁹ and gapless superconducting state⁴⁰ in proximitized altermagnets has also been predicted in a number of interesting theoretical studies. Unconventional superconductivity in altermagnetic metals with spin-orbit coupling has been addressed^{41,42}. Josephson effect^{43–46} and Andreev reflection^{47,48} in altermagnets have been discussed.

In this work, we would like to examine the existence of the FFLO state in a d-wave altermagnetic metal with attractive s-wave interaction at a given particle density. This fixed particle density removes a slight but potentially important difference in the setups considered in the previous two studies, if we seriously take into account the very fragile nature of the FFLO state.

Our results are briefly summarized by a rich phase diagram in Fig. 1, in the plane of the altermagnetic cou-

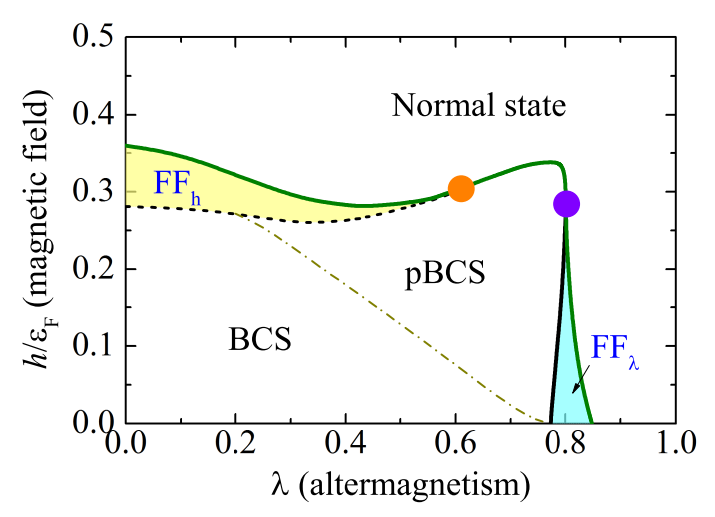


FIG. 1. The phase diagram at the binding energy $\varepsilon_B=0.08\varepsilon_F$ and at a negligible temperature $T=0.01T_F$. Two different FF phases, mainly driven by magnetic field (i.e., the FF_h phase) and by altermagnetism (see the FF_{\(\text{\gamma}\)} phase), are shown by the yellow and blue areas, respectively. The transition from the BCS phase to the FF_h phase is first order, as denoted by the dashed line. All the other transitions are second order and are shown by solid lines. The two dots indicate the two quantum tri-critical Lifshitz points, where the BCS, FF and normal states meet together. The dot-dashed line divides the BCS phase into two parts, a spin-population balanced BCS state (with imbalance $\delta n = (n_{\uparrow} - n_{\downarrow}) < 0.001n$) and a spin-population partially polarized BCS state. The latter is abbreviated as the pBCS state.

pling strength (i.e., λ in the horizontal axis) and the magnetic field (h in the vertical axis). On the one hand, at large altermagnetic coupling we confirm the altermagnetism induced FFLO state in the presence of attractive s-wave interaction, as observed by Hong, Park and Kim without magnetic field³⁸. We also confirm the smooth phase transitions from the BCS state to the FFLO state, and eventually to the normal state. Our extended study with the inclusion of magnetic field further reveals a nontrivial quantum tri-critical Lifshitz point^{49–51}, where two second-order phase transition curves intersect. On the other hand, at small altermagnetic coupling we find the usual magnetic field induced FFLO state¹⁸ and the transition from the BCS state to the FFLO is first order. This inevitably leads to another quantum Lifshitz point, where a first-order phase transition line meets a secondorder phase transition line. The existence of two quantum Lifshitz points clearly suggests that the FFLO states induced by magnetic field and altermagnetism are fundamentally different.

Remarkably, in the phase diagram we also find a large phase space for a polarized BCS superconductivity near the absolute zero temperature. This unexpected polarized BCS state might be understood as the reminiscence of the long-sought Sarma phase²³, whose thermodynamic instability is efficiently cured by the altermagnetism. The direct transition from the polarized BCS state to the nor-

mal state is smooth and locates between the two quantum Lifshitz points.

The rest of the paper is organized as follows. In the next chapter (Sec. II), we outline the model Hamiltonian that describes a d-wave altermagnetic metal in external magnetic field. In Sec. III, we briefly discuss how to solve the model Hamiltonian by using the standard mean-field theory, with an inhomogeneous FF order parameter. In Sec. IV. we present some details of our numerical calculations, which could be useful to improve the numerical accuracy. In Sec. V, we discuss in detail the two distinct kinds of the FF states driven by external magnetic field and altermagnetism, respectively. We show the existence of a polarized BCS phase due to the combined effect of magnetic field and altermagnetism. We also determine the nature of phase transitions between different states. Finally, we conclude in Sec. VI and present some outlooks for future works.

II. MODEL HAMILTONIAN

Let us start from the following model Hamiltonian for a two-dimensional Fermi system with the d-wave altermagnetic term³³ $J_{\mathbf{k}} \equiv \lambda \hbar^2 k_x k_y/(2m)$ and external magnetic field h along z-direction, $\mathcal{H} = \int d\mathbf{x} (\mathcal{H}_0 + \mathcal{H}_{int})$, where the Hamiltonian densities are,

$$\mathcal{H}_{0} = \sum_{\sigma=\uparrow,\downarrow} \psi_{\sigma}^{\dagger}(\mathbf{x}) \left[\hat{\xi}_{\mathbf{k}} + s(\sigma) \left(\hat{J}_{\mathbf{k}} + h \right) \right] \psi_{\sigma}(\mathbf{x}), (1)$$

$$\mathcal{H}_{int} = U_0 \psi_{\uparrow}^{\dagger}(\mathbf{x}) \psi_{\downarrow}^{\dagger}(\mathbf{x}) \psi_{\downarrow}(\mathbf{x}) \psi_{\uparrow}(\mathbf{x}). \tag{2}$$

Here, we have defined the operators $\hat{\xi}_{\mathbf{k}} \equiv -\hbar^2 \nabla^2/(2m) - \mu$, $\hat{k}_x = -i\partial_x$, $\hat{k}_y = -i\partial_y$ and $\hat{J}_{\mathbf{k}} \equiv \lambda \hbar^2 \hat{k}_x \hat{k}_y/(2m)$, and have denoted $s(\uparrow) = +1$ and $s(\downarrow) = -1$. The dimensionless parameter λ characterizes the strength of altermagnetism. The chemical potential μ in $\hat{\xi}_{\mathbf{k}}$ can be tuned to yield the given total particle density $n = n_{\uparrow} + n_{\downarrow}$. The Fermi system may or may not have a nonzero spin-population imbalance $\delta n = n_{\uparrow} - n_{\downarrow}$, depending on its ground state in the phase diagram.

For the inter-particle interaction, we consider a short-range s-wave contact potential. In two dimensions, its interaction strength U_0 can be conveniently regularized by using a two-body binding energy ε_B^{52} :

$$\frac{1}{U_0} = -\frac{1}{\mathcal{S}} \sum_{\mathbf{k}} \frac{1}{\hbar^2 k^2 / m + \varepsilon_B},\tag{3}$$

where S is the area of the Fermi system.

We note that, our model Hamiltonian provides an excellent description of some recently discovered unconventional magnets, particularly ${\rm RuO_2}^{29,36}$, although its classification as an altermagnet is still under debate. The model Hamiltonian is also potentially within reach in cold-atom laboratories⁵³. By loading a spin-1/2 Fermi gas of fermionic atoms into a specifically designed two-dimensional lattice, d-wave altermagnetism may arise

due to the Hubbard on-site repulsion⁵³. In addition, the external magnetic field can be introduced by tuning the imbalance between the two spin populations and an effective short-range attraction between fermions can be mediated by doping some bosonic atoms⁵⁴.

III. MEAN-FIELD THEORY

To search for the FF superconductivity, we assume a FF-like order parameter $\Delta(\mathbf{x}) = -U_0 \langle \psi_{\downarrow}(\mathbf{x}) \psi_{\uparrow}(\mathbf{x}) \rangle = \Delta \exp[i\mathbf{q} \cdot \mathbf{x}]$ and consider the standard mean-field decoupling of the interaction Hamiltonian density^{9,14},

$$\mathcal{H}_{int} \simeq -\left[\Delta(\mathbf{x})\psi_{\uparrow}^{\dagger}(\mathbf{x})\psi_{\downarrow}^{\dagger}(\mathbf{x}) + \text{H.c.}\right] - \frac{1}{U_0} \left|\Delta(\mathbf{x})\right|^2. \tag{4}$$

The direction of the FF momentum \mathbf{q} is determined by the altermagnetism. It can be either along the x-axis or along the y-axis, due to the $C_{4z}\mathcal{T}$ symmetry of the altermagnetic term³⁸. Here, we choose the x-axis for concreteness and set $\mathbf{q} = q\mathbf{e}_x$ and $\Delta(\mathbf{x}) = \Delta \exp[iqx]$. In the framework of the mean-field Bogoliubov-de Gennes (BdG) theory, the total Hamiltonian can be rewritten into the form^{9,14},

$$\mathcal{H}_{MF} = \int d\mathbf{x} \Phi^{\dagger}(\mathbf{x}) \,\mathcal{H}_{BdG} \Phi(\mathbf{x}) - \frac{\Delta^{2}}{U_{0}} \mathcal{S} + \mathcal{E}_{0}, \quad (5)$$

where $\Phi(\mathbf{x}) \equiv [\psi_{\uparrow}(\mathbf{x}), \psi_{\downarrow}^{\dagger}(\mathbf{x})]^T$ is the Nambu spinor and

$$\mathcal{H}_{BdG} \equiv \begin{bmatrix} \hat{\xi}_{\mathbf{k}} + \hat{J}_{\mathbf{k}} + h & -\Delta(\mathbf{x}) \\ -\Delta^*(\mathbf{x}) & -\hat{\xi}_{\mathbf{k}} + \hat{J}_{\mathbf{k}} + h \end{bmatrix}, \qquad (6)$$

and $\mathcal{E}_0' = \sum_{\mathbf{k}} (\hat{\xi}_{\mathbf{k}} - \hat{J}_{\mathbf{k}} - h)$ is an energy shift (to be specified below), due to the abnormal order in the field operators $\psi_{\downarrow}(\mathbf{x})$ and $\psi_{\downarrow}^{\dagger}(\mathbf{x})$ taken in the Nambu spinor representation.

A. Bogoliubov quasiparticles

As the FF order parameter takes a plane-wave form, it is convenient to diagonalize the mean-field Hamiltonian in momentum space, with the following Bogoliubov equations¹⁴,

$$\mathcal{H}_{BdG}\Phi_{\mathbf{k}}\left(\mathbf{x}\right) = E_{\mathbf{k}}\Phi_{\mathbf{k}}\left(\mathbf{x}\right),\tag{7}$$

where

$$\Phi_{\mathbf{k}}(\mathbf{x}) \equiv \begin{bmatrix} u_{\mathbf{k}\uparrow} e^{+iqx/2} \\ v_{\mathbf{k}\downarrow} e^{-iqx/2} \end{bmatrix} e^{i\mathbf{k}\mathbf{x}}$$
(8)

and $E_{\mathbf{k}}$ are the wavefunction and energy of the Bogoliubov quasiparticles, respectively. With this wavefunction, the energy shift is $\mathcal{E}_0' = \sum_{\mathbf{k}} (\xi_{\mathbf{k}-\mathbf{q}/2} - J_{\mathbf{k}-\mathbf{q}/2} - h)$, where $\xi_{\mathbf{k}} \equiv \hbar^2 k^2 / (2m) - \mu$, and the Bogoliubov equations recast into the form,

$$[\mathcal{H}_{BdG}] \begin{bmatrix} u_{\mathbf{k}\uparrow} \\ v_{\mathbf{k}\downarrow} \end{bmatrix} = E_{\mathbf{k}} \begin{bmatrix} u_{\mathbf{k}\uparrow} \\ v_{\mathbf{k}\downarrow} \end{bmatrix}, \tag{9}$$

where $[\mathcal{H}_{BdG}]$ is a 2 by 2 matrix given by,

$$\begin{bmatrix} \xi_{\mathbf{k}+\mathbf{q}/2} + J_{\mathbf{k}+\mathbf{q}/2} + h & -\Delta \\ -\Delta & -\xi_{\mathbf{k}-\mathbf{q}/2} + J_{\mathbf{k}-\mathbf{q}/2} + h \end{bmatrix}. \quad (10)$$

By diagonalizing the matrix $[\mathcal{H}_{BdG}]$, we thus obtain the two branches of the eigenvectors $[u_{\mathbf{k}\uparrow}^{(\eta)}, v_{\mathbf{k}\downarrow}^{(\eta)}]^T$ and eigenvalues $\eta E_{\mathbf{k}\eta}$, labeled by the index $\eta = \pm$. Explicitly, we have the single-particle excitation spectrum,

$$E_{\mathbf{k}\pm} = \sqrt{A_{\mathbf{k}}^2 + \Delta^2} \pm B_{\mathbf{k}},\tag{11}$$

where

$$A_{\mathbf{k}} \equiv \xi_{\mathbf{k}} + \frac{\hbar^2 q^2}{8m} + \lambda \frac{\hbar^2 q k_y}{4m},\tag{12}$$

$$B_{\mathbf{k}} \equiv \frac{\hbar^2 q k_x}{2m} + J_{\mathbf{k}} + h. \tag{13}$$

Here, as usual we have reversed the sign for the eigenvalue $-E_{\mathbf{k}-}$, in order to write the corresponding field operators of Bogoliubov quasiparticles $\alpha_{\mathbf{k}-}$ and $\alpha_{\mathbf{k}-}^{\dagger}$ in the normal order. This introduces another energy shift $\mathcal{E}_0'' = -\sum_{\mathbf{k}} E_{\mathbf{k}-}$ in the mean-field Hamiltonian. In the absence of altermagnetism or external magnetic field, our expression of the single-particle excitation spectrum recovers the results in Ref.¹⁸ and Ref.³⁸, respectively. In the end, we obtain the diagonalized mean-field Hamiltonian,

$$\mathcal{H}_{MF} = \sum_{\mathbf{k}\eta = \pm} E_{\mathbf{k}\eta} \alpha_{\mathbf{k}\eta}^{\dagger} \alpha_{\mathbf{k}\eta} - \frac{\Delta^2}{U_0} \mathcal{S} + \mathcal{E}_0, \qquad (14)$$

where

$$\mathcal{E}_0 = \mathcal{E}_0' + \mathcal{E}_0'' = \sum_{\mathbf{k}} \left(A_{\mathbf{k}} - \sqrt{A_{\mathbf{k}}^2 + \Delta^2} \right). \tag{15}$$

B. Thermodynamic potential

From the diagonalized Hamiltonian, we can straightforwardly write down the grand thermodynamic potential,

$$\Omega = -\frac{\Delta^2}{U_0} \mathcal{S} + \mathcal{E}_0 - k_B T \sum_{\mathbf{k}n = +} \ln\left(1 + e^{-\frac{E_{\mathbf{k}\eta}}{k_B T}}\right), \quad (16)$$

where the last term is the standard contribution of non-interacting fermionic particles to the thermodynamic potential. For given chemical potential μ and temperature T, we have two independent parameters: the order parameter Δ and the FF momentum q. These two parameters should be determined by minimizing the grand thermodynamic potential, i.e.,

$$\frac{\partial \Omega}{\partial \Delta} = 0, \tag{17}$$

$$\frac{\partial\Omega}{\partial q} = 0. ag{18}$$

Moreover, we need to satisfy the number equation,

$$n = \frac{k_F^2}{2\pi} = -\frac{\partial\Omega}{\partial\mu},\tag{19}$$

where k_F is the Fermi wavevector.

IV. NUMERICAL CALCULATIONS

In our numerical calculations, we typically take the Fermi wavevector k_F and Fermi energy ε_F as the units for wavevector and energy, respectively. This means that we can directly set $2m = \hbar = k_B = k_F = \varepsilon_F = 1$. In the dimensionless form, we find that the grand thermodynamic potential is given by $(k_x = k \cos \varphi \text{ and } k_y = k \sin \varphi)$,

$$\frac{\Omega}{\mathcal{S}k_F^2\varepsilon_F} = \frac{1}{4\pi^2} \int_0^{2\pi} d\varphi \left[\int_0^{k_c} dk C(k,\varphi) + \frac{c_1(\varphi)}{k_c} + \frac{c_2(\varphi)}{2k_c^2} + \cdots \right],\tag{20}$$

where

$$C(k,\varphi) = k \left[\frac{\Delta^2}{2k^2 + \varepsilon_B} + A_{\mathbf{k}} - \sqrt{A_{\mathbf{k}}^2 + \Delta^2} - T \sum_{\eta = \pm} \ln\left(1 + e^{-\frac{E_{\mathbf{k}\eta}}{T}}\right) \right]$$
(21)

and

$$A_{\mathbf{k}} = k^2 - \mu + \frac{q^2}{4} + \frac{\lambda q k \sin \varphi}{2},\tag{22}$$

$$E_{\mathbf{k}\pm} = \sqrt{A_{\mathbf{k}}^2 + \Delta^2} \pm \left(qk \cos \varphi + \frac{\lambda k^2 \sin 2\varphi}{2} + h \right). \tag{23}$$

Here, we have replaced the bare interaction strength U_0 by the binding energy ε_B ,

$$-\frac{\Delta^2}{U_0} = \frac{1}{4\pi^2} \int_0^{2\pi} d\varphi \int_0^{\infty} dkk \left[\frac{\Delta^2}{2k^2 + \varepsilon_B} \right]. \tag{24}$$

Furthermore, to accurately calculate the integral over $C(k,\varphi)$, we have introduced a high-momentum cut-off, i.e., $k_c \sim 10k_F$. Above k_c , we numerically expand,

$$C(k,\varphi) = \frac{c_1(\varphi)}{k^2} + \frac{c_2(\varphi)}{k^3} + \cdots$$
 (25)

The two coefficients $c_1(\varphi)$ and $c_2(\varphi)$ can be found numerically by a linear curve fitting. We first calculate

$$y_1 = k_1^3 C(k_1, \varphi),$$
 (26)

$$y_2 = k_2^3 C(k_2, \varphi),$$
 (27)

where, for example, $k_1 = k_c \gg 1$ and $k_2 = 2k_c \gg 1$. Then, we obtain,

$$c_1(\varphi) = \frac{y_1 - y_2}{k_1 - k_2},\tag{28}$$

$$c_2(\varphi) = \frac{y_2 k_1 - y_1 k_2}{k_1 - k_2}. (29)$$

A. Numerical procedure

To find all the possible phases, for a given set of parameters, including altermagnetic coupling λ , Zeeman field

 h/E_F , interaction parameter $\varepsilon_B/\varepsilon_F$, and temperature $T/(\varepsilon_F/k_B)$, we minimize the thermodynamic potential against Δ and q. As a simple and quick method, we shall use the Newton's gradient approach. The various derivatives can be approximated by numerical differences. This approach is efficient, provided a good guess of the initial parameters for Δ and q, which may be obtained by looking at the contour plot of the grand thermodynamic potential.

We try three different phases: the normal gas, BCS state and FF state. Once these phases are determined, we calculate their free energy per particle, $F/N = \Omega/N + \mu$, where $N = n\mathcal{S}$ is the total number of particles. By comparing the free energy, we finally determine which one is the ground state and then construct the whole phase diagram.

V. RESULTS AND DISCUSSIONS

In our numerical calculations, we always include a negligible temperature $T=0.01T_F$, to soften the sharp Fermi surface at zero temperature and hence to improve the numerical accuracy. We take a typical binding energy $\varepsilon_B=0.08\varepsilon_F$, which leads to a BCS pairing gap $\Delta_0=\sqrt{2\varepsilon_B\varepsilon_F}=0.4\varepsilon_F$ and a chemical potential $\mu_0=\varepsilon_F-\varepsilon_B/2=0.96\varepsilon_F$ in the absence of altermagnetism and magnetic field⁵².

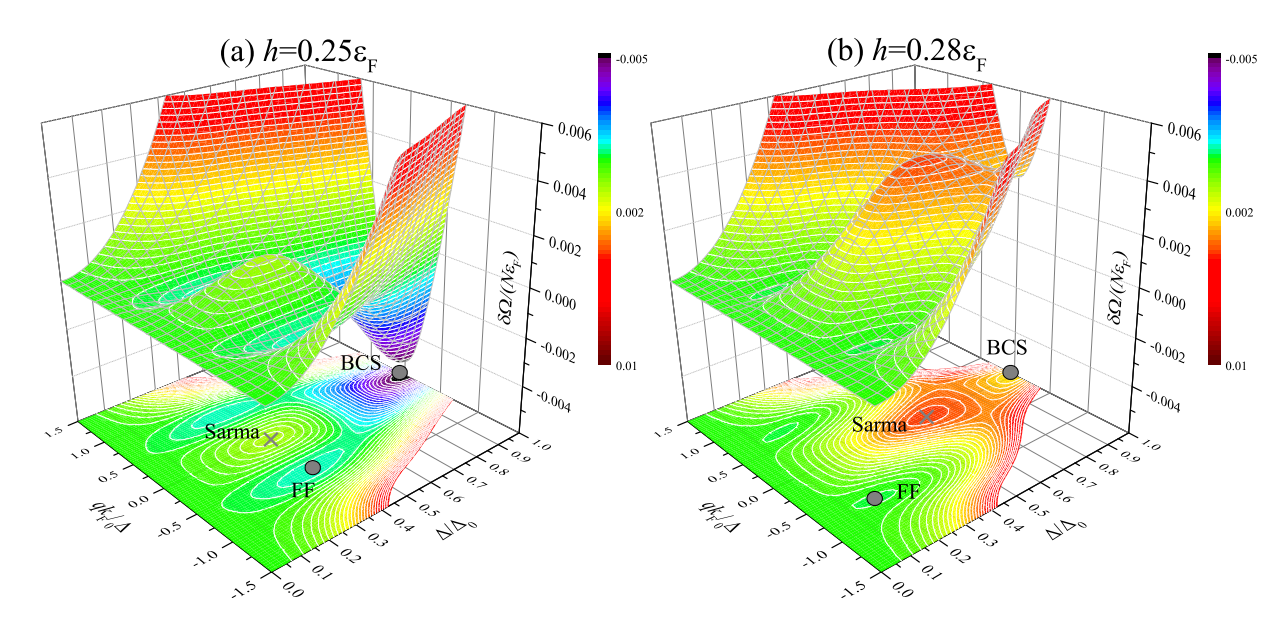


FIG. 2. The landscape of the thermodynamic potential $(\Omega - \Omega_0)/(N\varepsilon_F)$, as a function of the pairing amplitude Δ and the FF momentum q, at two magnetic fields: $h = 0.25\varepsilon_F$ (a) and $h = 0.28\varepsilon_F$ (b). Here, Ω_0 is the thermodynamic potential of the reference normal state and we denote $\delta\Omega \equiv \Omega - \Omega_0$. The different candidate phases are highlighted in the contour plot shown at the bottom. We take a small altermagnetic coupling constant $\lambda = 0.2$ and fix the chemical potential $\mu = \mu_0 = 0.96\varepsilon_F$. The pairing amplitude Δ and the FF momentum are measured in units of Δ_0 and Δ_0/k_F , respectively, where $\Delta_0 = 0.4\varepsilon_F$ at the binding energy $\varepsilon_B = 0.08\varepsilon_F$.

A. The FF state driven by magnetic field

We first consider the conventional case, where the inhomogeneous FFLO state is driven by magnetic field. In the absence of altermagnetism (i.e., $\lambda=0$), for our chosen binding energy the first-order phase transition from the BCS state to the FF state at zero temperature is analytically known to occur¹⁸ at $h_{FF}=(\varepsilon_B/2)\sqrt{1+4\mu_0/\varepsilon_B}=0.28\varepsilon_F$. The next transition from the FF state to a normal gas occurs¹⁸ at $h_c=\sqrt{2\mu\varepsilon_B-\varepsilon_B^2}\sim 0.39\varepsilon_F$.

In Fig. 2, we show the landscape of the thermodynamic potential $(\Omega - \Omega_0)/(N\varepsilon_F)$ in the $q - \Delta$ plane at two magnetic fields and in the presence of a small altermagnetic coupling constant $\lambda = 0.2$. We have subtracted the non-interacting thermodynamic potential Ω_0 , so the preference of the BCS state and the FF state over the normal state should be evident. Typically, we find three candidate phases⁹, two are local minima (i.e., BCS at q = 0 and FF at $q \neq 0$) and one is a local maximum (i.e., Sarma at q = 0). Here, it is worth noting that the landscape is symmetric with respect to q (or more precisely q_x in our choice of the FF momentum) and we only need to consider the FF state located at q > 0.

At the magnetic field $h = 0.25\varepsilon_F$ (see Fig. 2(a)), the BCS state is clearly the absolute ground state. By increasing magnetic field above the critical field h_{FF} , whose value is slightly smaller than $0.28\varepsilon_F$ due to the existence of the small altermagnetic coupling $\lambda = 0.2$, the FF state becomes more favorable, as illustrated in Fig. 2(b). The transition from the BCS state to the FF state should be first order, as the two corresponding local minima are

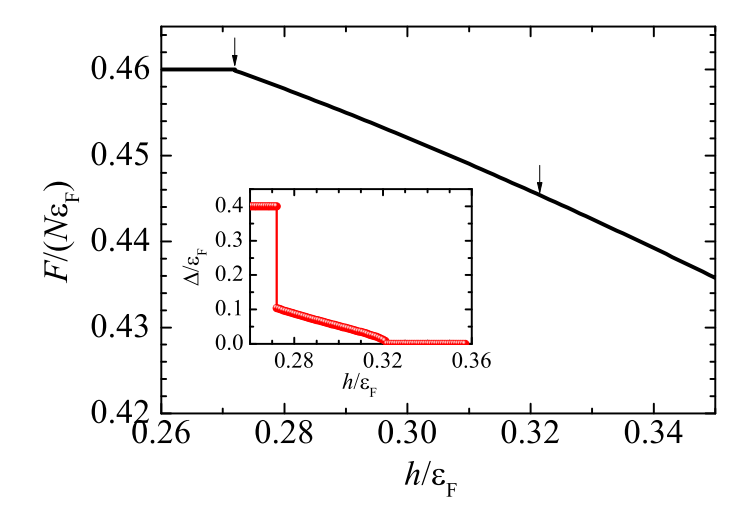


FIG. 3. The free energy $F/(N\varepsilon_F)$ as a function of magnetic field, at a small alternagnetic coupling constant $\lambda=0.2$. The two arrows indicate the transitions from the BCS state to the FF_h state and finally to the normal state. The inset shows the pairing gap Δ as a function of the magnetic field.

well separated by an energy barrier (see, i.e., the saddle point near the local Sarma maximum).

In Fig. 3, we report the free energy per particle as a function of magnetic field, in the presence of the small altermagnetic coupling constant $\lambda=0.2$. The free energy exhibits a kink at $h_{FF}\simeq 0.272\varepsilon_F$, as a result of the first-order phase transition from the BCS state to the FF state. This is in line with a sudden decrease in the

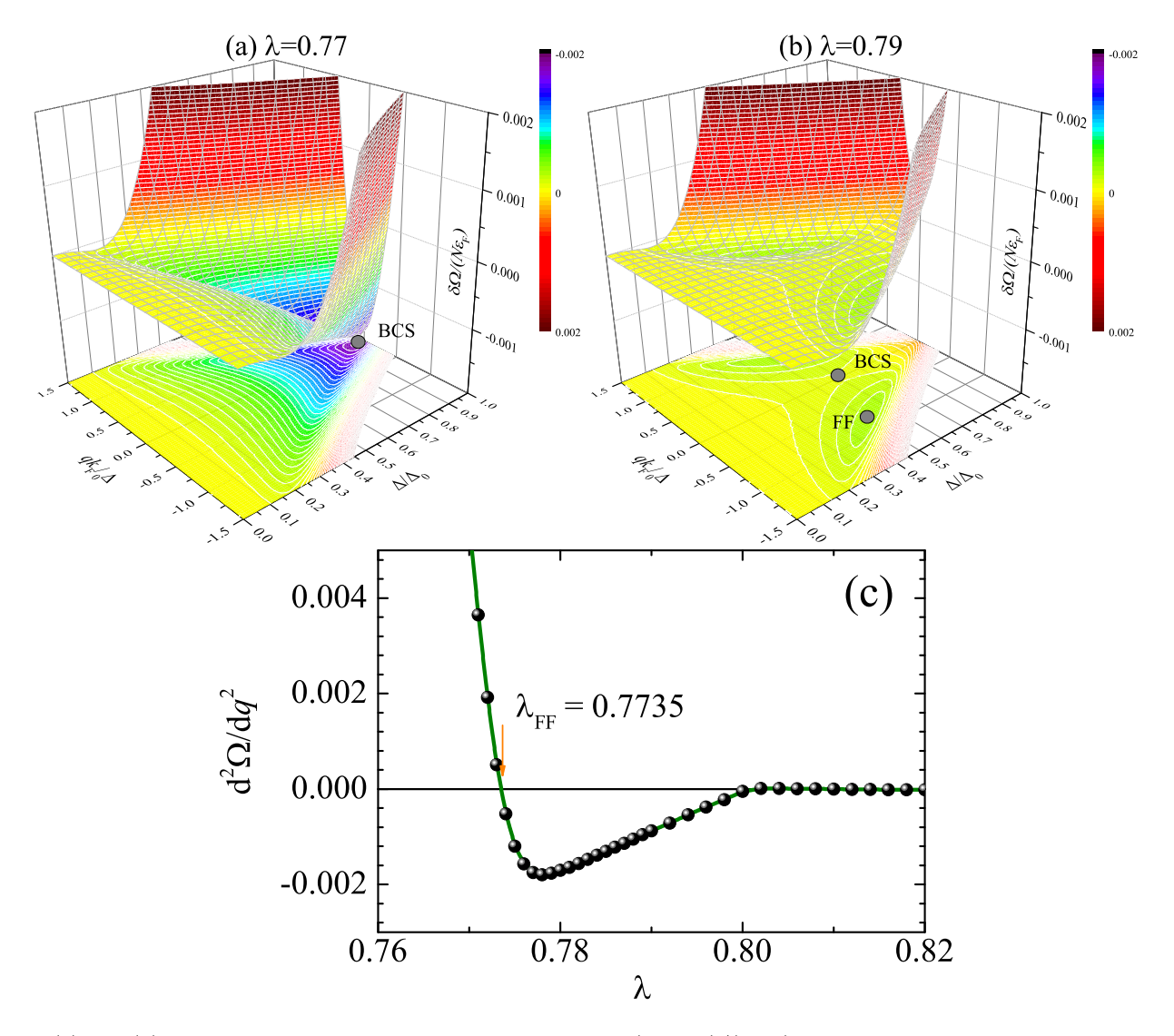


FIG. 4. (a) and (b) The landscape of the thermodynamic potential $(\Omega - \Omega_0)/(N\varepsilon_F)$, as a function of the pairing amplitude Δ and the FF momentum q, at two altermagnetic coupling constants: $\lambda = 0.77$ and $\lambda = 0.79$, in the absence of magnetic field (h = 0). At the bottom of the two subfigures, we explicitly show the BCS and FF phases in the contour plot. We have fixed the chemical potential $\mu = 0.92831\varepsilon_F$. (c) The instability of the BCS solution towards the FFLO state, as signaled by the condition $\partial\Omega^2/\partial q^2 < 0$. The quantity $\partial\Omega^2/\partial q^2$ is shown in units of $\mathcal{S}\varepsilon_F^2$. The FFLO instability sets in at $\lambda > \lambda_{FF} \simeq 0.7735$.

pairing gap Δ , as shown in the inset. By further increasing magnetic field, the pairing gap eventually vanishes at $h_c \simeq 0.322\varepsilon_F$, giving a smooth second-order transition to the normal state.

We repeat the calculation of the free energy for other values of the altermagnetic coupling constant λ and determine how the parameter window of the FF_h phase changes. Here, the subscript "h" is used to indicate that the FF state is driven by magnetic field. As shown in the phase diagram Fig. 1 (see the yellow area), the FF_h phase window shrinks with increasing λ . Eventually, the first-order transition line and the second-order transition line meet at a quantum tri-critical Lifshitz point, located at about $(\lambda, h) = (0.57, 0.292\varepsilon_F)$. A similar tri-critical point for the FFLO phase is known to appear in a classical way by increasing temperature¹.

B. The FF state driven by altermagnetism

We now turn to consider the appearance of the FF state at the large altermagnetic coupling. In Fig. 4, we present the landscape of the thermodynamic potential $(\Omega - \Omega_0)/(N\varepsilon_F)$ at the two altermagnetic coupling constants $\lambda = 0.77$ and $\lambda = 0.79$, without magnetic field. At $\lambda = 0.77$ (see Fig. 4(a)), we find only a global minimum at zero momentum with a pairing gap $\Delta = \Delta_0$, corresponding to the standard BCS state. By increasing λ from 0.77 to 0.79, it turns out that such as global minimum is rapidly lifted up and turns into a saddle point with the pairing gap $\Delta < \Delta_0$. As illustrated in Fig. 4(b), such a saddle point, which we still refer to as a BCS solution, suffers from an instability towards a nearby min-

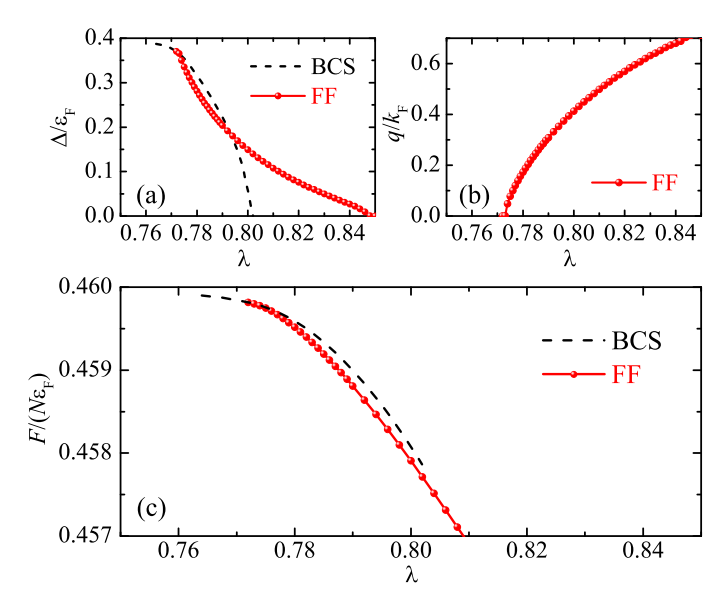


FIG. 5. The pairing gap Δ/Δ_0 , the FF momentum q/k_F , and the free energy $F/(N\varepsilon_F)$ of the BCS state and the FFLO state, as a function of the altermagnetic coupling constant, in the absence of magnetic field (h=0).

imum at $q \neq 0$. This minimum is precisely the FF state driven by altermagnetism, found earlier by Hong, Park and Kim in Ref.³⁸, although there is no net magnetic field in the d-wave altermagnetic term.

In sharp contrast to the case of a large magnetic field, we observe that a large altermagnetism does not introduce a local maximum in the landscape of the thermodynamic potential, which acts as an energy barrier for competing phases. Moreover, the FF state arises only after the BCS solution gradually changes into a saddle point, with $\partial\Omega^2/\partial q^2<0$. Therefore, the phase transition from the BCS state to the FF state is smooth. To confirm this observation, in Fig. 4(c) we plot the quantity $\partial\Omega^2/\partial q^2$ with increasing altermagnetic coupling constant λ . Indeed, we find that $\partial\Omega^2/\partial q^2$ changes its sign at a critical altermagnetic coupling $\lambda_{FF}=0.773$. Beyond this critical value, the FF state becomes the absolute ground state.

The above instability analysis is useful to accurately determine the critical altermagnetic coupling λ_{FF} . However, it does not help to locate another phase transition point λ_c from the FF state to the normal state, since the metastable BCS solution ceases to exist once $\lambda > 0.8$. To determine the critical altermagnetic coupling λ_c , we calculate the pairing gap and the free energy of the altermagnetism-driven FF state and compare them with the corresponding BCS results in Fig. 5(a) and Fig. 5(c), respectively.

As expected, as a result of the second-order phase transition, the FF pairing gap smoothly connect to the BCS pairing gap at λ_{FF} . The two free energies also smooth connect. Furthermore, the FF momentum becomes nonzero precisely at λ_{FF} (see Fig. 5(b))³⁸. On the other hand, the value of the critical altermagnetic

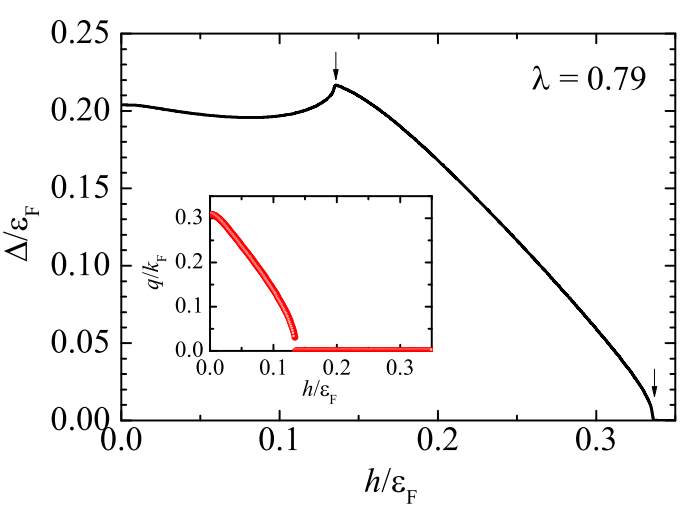


FIG. 6. The pairing gap Δ (main figure) and the FF momentum q (inset), as a function of the magnetic field, at a large altermagnetic coupling constant $\lambda=0.79$. The two arrows indicate the second-order phase transitions from the FF $_{\lambda}$ state to the polarized BCS state and finally to the normal state.

coupling $\lambda_c \simeq 0.848$ can be extracted by tracing the FF pairing gap to vanish. Therefore, without magnetic field (h=0), the altermagnetic metal with a two-body binding energy $\varepsilon_B=0.08\varepsilon_F$ is an inhomogeneous FF superconductor in a relatively narrow region, $0.773 < \lambda < 0.848$.

To investigate how the altermagnetism-driven FF state is affected by magnetic field, in Fig. 6 we present the pairing gap (main figure) and the FF momentum (inset) of the ground state, as a function of magnetic field. At zero magnetic field (h = 0), the Fermi system is initially in the FF state with a pairing gap $\Delta \simeq 0.2\varepsilon_F$ and a FF momentum $q \simeq 0.3k_F$. By increasing magnetic field, we find the pairing gap of the FF ground state shows a non-monotonic dependence, up to a critical field $h_{FF} \simeq$ $0.135\varepsilon_F$. Beyond this critical value, the system turns into a BCS state. This smooth transition can be double checked by looking at the FF momentum q in the inset, which precisely vanishes at h_{FF} . By furthering increase the magnetic field, we find the pairing gap of the BCS state eventually becomes zero at the second critical field $h_c \simeq 0.336\varepsilon_F$ and the system becomes normal.

We perform the calculations at different altermagnetic couplings in the interval $0.773 < \lambda < 0.8$ and observe the similar magnetic field dependence. At another interval $0.8 < \lambda < 0.848$, the Fermi system turns out to directly transit from the FF state to the normal state at the critical field h_c . In the phase diagram Fig. 1, we highlight the parameter window of the FF $_{\lambda}$ phase with blue color, where the subscript " λ " now represents the altermagnetism-driven FF state. The window shrinks with increasing magnetic field and ends at a non-trivial quantum critical point $(\lambda, h) \simeq (0.80, 0.285\varepsilon_F)$, where the two second-order phase transition curves intersect

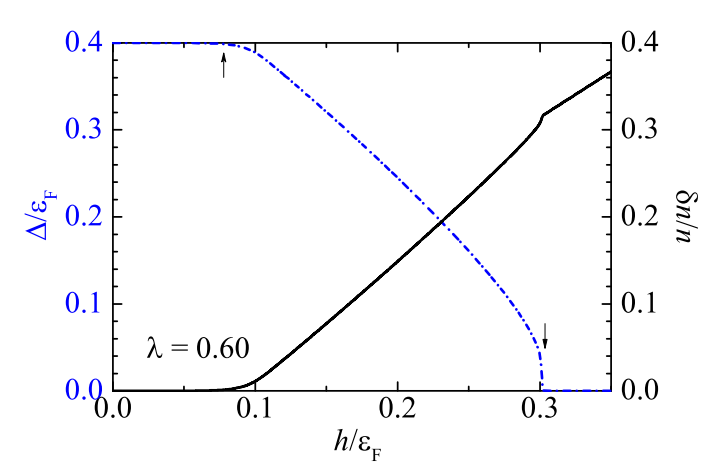


FIG. 7. The pairing gap Δ (left axis) and the spin-population imbalance δn (right axis), as a function of the magnetic field, at the altermagnetic coupling constant $\lambda=0.60$. The two arrows indicate the crossover from the BCS state to the polarized BCS state and the second-order phase transition from the polarized BCS state to the normal state, respectively.

(see the purple dot in the phase diagram).

C. The polarized BCS state

As the spin-population imbalance $\delta n = n_{\uparrow} - n_{\downarrow}$ of a FF state is nonzero, the continuous phase transition from the FF state to the BCS state shown in Fig. 6 at the critical field $h_{FF} \simeq 0.135\varepsilon_F$ is highly non-trivial. It is suggestive that the spin-population imbalance of the BCS state is also nonzero. Hence, we obtain a partially spin-population polarized BCS state as the ground state at zero temperature, which can hardly be realized in other interacting Fermi systems^{25,26}.

In fact, in the phase diagram Fig. 1 we find a large parameter window for the polarized BCS state. To be concrete, in Fig. 7 we show the pairing gap Δ and the spin-population imbalance δn of the ground state at the altermagnetic coupling $\lambda=0.6$, with increasing magnetic field. The pairing gap decreases from the constant value Δ_0 at a critical field $h_{\rm pBCS}\simeq 0.076\varepsilon_F$. At the same critical field, the spin-population imbalance δn becomes nonzero and starts to increase with magnetic field almost linearly.

At nearly zero temperature a nonzero spin-population imbalance can only be supported, when the single-particle excitation spectrum of the BCS state becomes gapless. To confirm this, in Fig. 8 we present the Bogoliubov spectrum $E_{\mathbf{k}-}$ at the two magnetic fields $h=0.05\varepsilon_F$ (a) and $h=0.15\varepsilon_F$ (b). In the former case, which is below the critical field $h_{\text{pBCS}}\simeq 0.076\varepsilon_F$, the spectrum is gapped, consistent with the fact that $\delta n\simeq 0$. In the latter case, we see clearly that the spectrum $E_{\mathbf{k}-}$ becomes gapless around the two diagonal points $(k_x,k_y)\sim [\pm k_F\cos(\pi/4),\pm k_F\sin(\pi/4)]$ in mo-

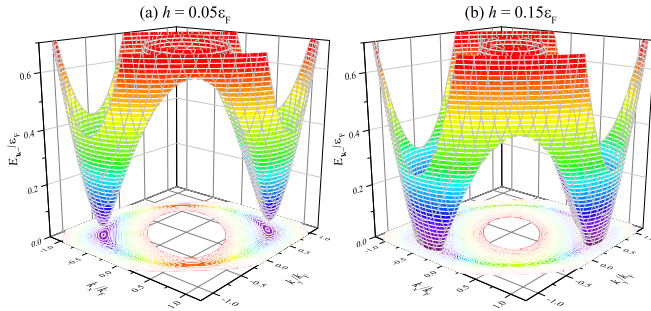


FIG. 8. The single-particle excitation spectrum $E_{\mathbf{k}-}$ of a BCS state at $h=0.05\varepsilon_F$ (a) and of a polarized BCS state at $h=0.15\varepsilon_F$, in the presence of an altermagnetic coupling $\lambda=0.60$. With increasing magnetic field, the excitation spectrum becomes gapless and supports a nonzero spin-population imbalance.

mentum space.

It is readily seen that we can use the gapless condition $E_{\mathbf{k}-} = 0$ at q = 0, or more explicitly,

$$h = \sqrt{(k^2 - \mu_0)^2 + \Delta_0^2} - \frac{\lambda k^2 \sin 2\varphi}{2}$$
 (30)

to estimate the critical field h_{pBCS} at a given altermagnetic coupling constant λ . By minimizing the right-hand-side of the equation with respect to k^2 and φ , we find that

$$h_{\text{pBCS}} = \frac{1}{2} \left[\sqrt{4 - \lambda^2 \Delta_0} - \lambda \mu_0 \right]. \tag{31}$$

This estimation seems to be consistent with our numerical calculation (i.e., see the dot-dashed line in Fig. 1). In particular, by setting $h_{\rm pBCS}=0$, we obtain a threshold altermagnetic coupling $\lambda_{\rm thres}=2\Delta_0/\sqrt{\Delta_0^2+\mu_0^2}\simeq 0.77$. This value agrees excellently well with the critical altermagnetic coupling $\lambda_{FF}=0.773$ at zero magnetic field.

Finally, in the weak coupling regime ($\varepsilon_B \ll \varepsilon_F$) that we are interested in, since the threshold coupling $\lambda_{\rm thres} \simeq 2\Delta_0/\varepsilon_F$ scales linearly with the BCS pairing gap Δ_0 , we anticipate that our phase diagram Fig. 1 qualitatively holds for other binding energies, aside from an overall rescaling in the energy scale.

VI. CONCLUSIONS AND OUTLOOKS

To conclude, we have investigated the inhomogeneous FFLO in an altermagnetic metal, driven by either external magnetic field or d-wave altermagnetism. We have confirmed the emergence of the FFLO state at large altermagnetic coupling in the presence of an s-wave interparticle attraction and thereby have clarified its formation mechanism, which is not reconciled in the recent two studies^{27,38}. We have also clarified the nature of quantum phase transitions occurring between competing phases and have constructed a universal rich phase diagram Fig. 1.

Quite unexpectedly, we have found a uniform, partially spin-populated polarized BCS state, due to the altermagnetic coupling term. This polarized BCS phase has a significant parameter space in the phase diagram. Due to its gapless single-particle excitation spectrum, we anticipate that very intriguing collective excitations would arise in the polarized BCS state. Its dynamic response and sound propagation would be an interesting topic for future studies 26,55 .

Furthermore, we have also identified the existence of two quantum tri-critical Lifshitz points^{49–51}. A

brief discussion of the related Lifshitz physics based on Ginzburg-Landau free-energy functional will be presented elsewhere 56 .

ACKNOWLEDGMENTS

This research was supported by the Australian Research Council's (ARC) Discovery Program, Grants Nos. DP240101590 (H.H.) and DP240100248 (X.-J.L.).

- ¹ R. Casalbuoni and G. Nardulli, Inhomogeneous superconductivity in condensed matter and QCD, Rev. Mod. Phys. **76**, 263 (2004).
- ² L. Radzihovsky and D. E. Sheehy, Imbalanced Feshbach-resonant Fermi gases, Rep. Prog. Phys. **73**, 076501 (2010).
- ³ K. B. Gubbels and H. T. C. Stoof, Imbalanced Fermi gases at unitarity, Phys. Rep. **525**, 255 (2013).
- ⁴ T. Kawamura and Y. Ohashi, Non-equilibrium BCS-BEC crossover and unconventional FFLO superfluid in a strongly interacting driven-dissipative Fermi gas, AAPPS Bull. **34**, 31 (2024).
- ⁵ P. Fulde and R. A. Ferrell, Superconductivity in a Strong Spin-Exchange Field, Phys. Rev. **135**, A550 (1964).
- ⁶ A. I. Larkin and Yu. N. Ovchinnikov, Nonuniform state of superconductors, Zh. Eksp. Teor. Fiz. 47, 1136 (1964) [Sov. Phys. JETP 20, 762 (1965)].
- ⁷ Y. Ohashi, On the Fulde–Ferrell State in Spatially Isotropic Superconductors, J. Phys. Soc. Jpn. **71**, 2625 (2002).
- ⁸ S. Uji, T. Terashima, M. Nishimura, Y. Takahide, T. Konoike, K. Enomoto, H. Cui, H. Kobayashi, A. Kobayashi, H. Tanaka, M. Tokumoto, E. S. Choi, T. Tokumoto, D. Graf, and J. S. Brooks, Vortex Dynamics and the Fulde-Ferrell-Larkin-Ovchinnikov State in a Magnetic-Field-Induced Organic Superconductor, Phys. Rev. Lett. 97, 157001 (2006).
- ⁹ H. Hu and X.-J. Liu, Mean-field phase diagrams of imbalanced Fermi gases near a Feshbach resonance, Phys. Rev. A 73, 051603(R) (2006).
- ¹⁰ H. Hu, X.-J. Liu, and P. D. Drummond, Phase Diagram of a Strongly Interacting Polarized Fermi Gas in One Dimension, Phys. Rev. Lett. 98, 070403 (2007).
- ¹¹ X.-J. Liu, H. Hu, and P. D. Drummond, Fulde-Ferrell-Larkin-Ovchinnikov states in one-dimensional spin-polarized ultracold atomic Fermi gases, Phys. Rev. A 76, 043605 (2007).
- M. Kenzelmann, Th. Strässle, C. Niedermayer, M. Sigrist, B. Padmanabhan, M. Zolliker, A. D. Bianchi, R. Movshovich, E. D. Bauer, J. L. Sarrao, and J. D. Thompson, Coupled superconducting and magnetic order in CeCoIn₅, Science 321, 1652 (2008).
- Y.-A. Liao, A. S. C. Rittner, T. Paprotta, W. Li, G. B. Partridge, R. G. Hulet, S. K. Baur, and E. J. Mueller, Nature (London) 467, 567 (2010).
- ¹⁴ X.-J. Liu and H Hu, Inhomogeneous Fulde-Ferrell superfluidity in spin-orbit-coupled atomic Fermi gases, Phys. Rev. A 87, 051608(R) (2013).
- ¹⁵ Y. Cao, S.-H. Zou, X.-J. Liu, S. Yi, G.-L. Long, and H. Hu,

- Gapless Topological Fulde-Ferrell Superfluidity in Spin-Orbit Coupled Fermi Gases, Phys. Rev. Lett. **113**, 115302 (2014).
- ¹⁶ S. Gerber, M. Bartkowiak, J. L. Gavilano, E. Ressouche, N. Egetenmeyer, C. Niedermayer, A. D. Bianchi, R. Movshovich, E. D. Bauer, J. D. Thompson, and M. Kenzelmann, Switching of magnetic domains reveals spatially inhomogeneous superconductivity, Nature Phys. 10, 126 (2014).
- M. Takahashi, T. Mizushima, and K. Machida, Multiband effects on Fulde-Ferrell-Larkin-Ovchinnikov states of Paulilimited superconductors, Phys. Rev. B 89, 064505 (2014).
- ¹⁸ D. E. Sheehy, Fulde-Ferrell-Larkin-Ovchinnikov state of two-dimensional imbalanced Fermi gases, Phys. Rev. A 92, 053631 (2015).
- J. Wang, Y. Che, L. Zhang, and Q. Chen, Instability of Fulde-Ferrell-Larkin-Ovchinnikov states in atomic Fermi gases in three and two dimensions, Phys. Rev. B 97, 134513 (2018).
- T. Kawamura and Y. Ohashi, Feasibility of a Fulde-Ferrell-Larkin-Ovchinnikov superfluid Fermi atomic gas, Phys. Rev. A 106, 033320 (2022).
- P. Wan, O. Zheliuk, N. F. Q. Yuan, X. Peng, L. Zhang, M. Liang, U. Zeitler, S. Wiedmann, N. E. Hussey, T. T. M. Palstra, and J. Ye, Orbital Fulde–Ferrell–Larkin–Ovchinnikov state in an Ising superconductor, Nature 619, 46 (2023).
- D. Zhao, L. Debbeler, M. Kühne, S. Fecher, N. Gross, and J. Smet, Evidence of finite-momentum pairing in a centrosymmetric bilayer, Nature Phys. 19, 1599 (2023).
- ²³ G. Sarma, On the influence of a uniform exchange field acting on the spins of the conduction electrons in a superconductor, J. Phys. Chem. Solids 24, 1029 (1963).
- ²⁴ W. V. Liu and F. Wilczek, Interior Gap Superfluidity, Phys. Rev. Lett. **90**, 047002 (2003).
- ²⁵ M. M. Forbes, E. Gubankova, W. V. Liu, and F. Wilczek, Stability Criteria for Breached-Pair Superfluidity, Phys. Rev. Lett. **94**, 017001 (2005).
- ²⁶ P. Zou, L. He, X.-J. Liu, and H. Hu, Strongly interacting Sarma superfluid near orbital Feshbach resonances, Phys. Rev. A 97, 043616 (2018).
- D. Chakraborty and A. M. Black-Schaffer, Zero-field finite-momentum and field-induced superconductivity in altermagnets, Phys. Rev. B 110, L060508 (2024).
- ²⁸ S. Hayami, Y. Yanagi, and H. Kusunose, Momentum-Dependent Spin Splitting by Collinear Antiferromagnetic Ordering, J. Phys. Soc. Jpn. 88, 123702 (2019).
- ²⁹ M. Uchida, T. Nomoto, M. Musashi, R. Arita, and M.

- Kawasaki, Superconductivity in uniquely strained RuO2 films, Phys. Rev. Lett. **125**, 147001 (2020).
- ³⁰ S. Hayami, Y. Yanagi, and H. Kusunose, Spontaneous antisymmetric spin splitting in noncollinear antiferromagnets without spin-orbit coupling, Phys. Rev. B **101**, 220403(R) (2020).
- S. Hayami, Y. Yanagi, and H. Kusunose, Bottom-up design of spin-split and reshaped electronic band structures in antiferromagnets without spin-orbit coupling: Procedure on the basis of augmented multipoles, Phys. Rev. B 102, 144441 (2020).
- ³² L. Šmejkal, R. González-Hernández, T. Jungwirth, and J. Sinova, Crystal time-reversal symmetry breaking and spontaneous Hall effect in collinear antiferromagnets, Sci. Adv. 6, eaaz8809 (2020).
- ³³ L. Šmejkal, J. Sinova, and T. Jungwirth, Emerging Research Landscape of Altermagnetism, Phys. Rev. X 12, 040501 (2022).
- ³⁴ I. I. Mazin, Notes on altermagnetism and superconductivity, arXiv:2203.05000 (2022).
- ³⁵ I. I. Mazin, Altermagnetism in MnTe: Origin, predicted manifestations, and routes to detwinning, Phys. Rev. B 107, L100418 (2023).
- M. Hiraishi, H. Okabe, A. Koda, R. Kadono, T. Muroi, D. Hirai, and Z. Hiroi, Nonmagnetic ground state in RuO2 revealed by muon spin rotation, Phys. Rev. Lett. 132, 166702 (2024).
- O. J. Amin, A. Dal Din, E. Golias, Y. Niu, A. Zakharov, S. C. Fromage, C. J. B. Fields, S. L. Heywood, R. B. Cousins, F. Maccherozzi, J. Krempaský, J. H. Dil, D. Kriegner, B. Kiraly, R. P. Campion, A. W. Rushforth, K. W. Edmonds, S. S. Dhesi, L. Šmejkal, T. Jungwirth, and P. Wadley, Nanoscale imaging and control of altermagnetism in MnTe, Nature 636, 348 (2024).
- ³⁸ S. Hong, M. J. Park, and K.-M. Kim, Unconventional p-wave and finite-momentum superconductivity induced by altermagnetism through the formation of Bogoliubov Fermi surface, Phys. Rev. B 111, 054501 (2025).
- ³⁹ S.-B. Zhang, L.-H. Hu, and T. Neupert, Finite-momentum Cooper pairing in proximitized altermagnets, Nat. Commun. 15, 1801 (2024).
- ⁴⁰ M. Wei, L. Xiang, F. Xu, L. Zhang, G. Tang, and J. Wang, Gapless superconducting state and mirage gap in altermagnets, Phys. Rev. B 109, L201404 (2024).
- ⁴¹ D. Zhu, Z.-Y. Zhuang, Z. Wu, and Z. Yan, Topological su-

- perconductivity in two-dimensional altermagnetic metals, Phys. Rev. B **108**, 184505 (2023).
- ⁴² V. S. de Carvalho and H. Freire, Unconventional superconductivity in altermagnets with spin-orbit coupling, Phys. Rev. B 110, L220503 (2024).
- ⁴³ J. A. Ouassou, A. Brataas, and J. Linder, dc Josephson effect in altermagnets, Phys. Rev. Lett. **131**, 076003 (2023).
- ⁴⁴ B. Lu, K. Maeda, H. Ito, K. Yada, and Y. Tanaka, φ Josephson Junction Induced by Altermagnetism, Phys. Rev. Lett. **133**, 226002 (2024).
- ⁴⁵ K. Maeda, B. Lu, K. Yada, and Y. Tanaka, Theory of Tunneling Spectroscopy in Unconventional p-Wave Magnet-Superconductor Hybrid Structures, J. Phys. Soc. Jpn. 93, 114703 (2024).
- ⁴⁶ Y. Fukaya, K. Maeda, K. Yada, J. Cayao, Y. Tanaka, and B. Lu, Josephson effect and odd-frequency pairing in superconducting junctions with unconventional magnets, Phys. Rev. B 111, 064502 (2025).
- ⁴⁷ M. Papaj, Andreev reflection at the altermagnetsuperconductor interface, Phys. Rev. B **108**, L060508 (2023).
- ⁴⁸ C. Sun, A. Brataas, and J. Linder, Andreev reflection in altermagnets, Phys. Rev. B 108, 054511 (2023).
- ⁴⁹ R. M. Hornreich M. Luban, and S. Shtrikman , Critical Behavior at the Onset of \overrightarrow{k} -Space Instability on the λ Line, Phys. Rev. Lett. **35**, 1678 (1975).
- ⁵⁰ K. B. Gubbels, J. E. Baarsma, and H. T. C. Stoof, Lifshitz Point in the Phase Diagram of Resonantly Interacting ⁶Li-⁴⁰K Mixtures, Phys. Rev. Lett. **103**, 195301 (2009).
- ⁵¹ R. D. Pisarski, V. V. Skokov, and A. M. Tsvelik, A pedagogical introduction to the Lifshitz regime, Universe 5, 48 (2019).
- ⁵² L. He, H. Lü, G. Cao, H. Hu, and X.-J. Liu, Quantum fluctuations in the BCS-BEC crossover of two-dimensional Fermi gases, Phys. Rev. A 92, 023620 (2015).
- ⁵³ P. Das, V. Leeb, J. Knolle, and M. Knap, Realizing Altermagnetism in Fermi-Hubbard Models with Ultracold Atoms, Phys. Rev. Lett. **132**, 263402 (2024).
- ⁵⁴ B. J. DeSalvo, K. Patel, G. Cai, and C. Chin, Observation of fermion-mediated interactions between bosonic atoms, Nature (London) **568**, 61 (2019).
- ⁵⁵ H. Hu, E. Taylor, X.-J. Liu, S. Stringari, and A. Griffin, Second sound and the density response function in uniform superfluid atomic gases, New J. Phys. **12**, 043040 (2010).
- ⁵⁶ H. Hu and X.-J. Liu, Quantum Lifshitz points in an altermagnetic metal, arXiv:2505.10242v1 (2025).